Chapter 6

Critical Fields

In this chapter we discuss in detail how the Ginzburg-Landau theory allows to determine the critical magnetic fields for both type I and type II superconductors. This represents an interesting application of the Ginzburg-Landau theory, which is of practical use.

In order to simplify the considerations we assume that the superconducting probe has the shape of a long stretched cylinder. According to the discussion in Subsection 2.4.2 it is then justified to neglect effects originating from any stray field as the corresponding demagnetization factor vanishes.

6.1 Overview

According to Chapter 2 type I and type II superconductors differ in their respective magnetization curves, see Fig. 6.1. They are characterized by the respective critical fields, which we summarize briefly as follows:

- The Meissner-Ochsenfeld effect, that the magnetic induction is completely expelled from the superconductor, starts to become no longer valid at the critical field H_{c1}. To this end the first flux quanta enter the volume of the superconductor. The centers of flux quanta are normal conducting, so the magnetic induction is non-vanishing there.
- Then at the critical field H_{c2} the whole superconductor consists of flux quanta. But superconductivity still persists at the surface.
- And, finally, at the critical field H_{c3} also the surface superconductivity breaks down.

For superconductors of type II it is possible to define a thermodynamic critical magnetic field H_c^{th} as follows. To this end one applies a Maxwell construction, which generically occurs for phase transitions of first order. Namely, one considers the magnetization energy of type II

a) 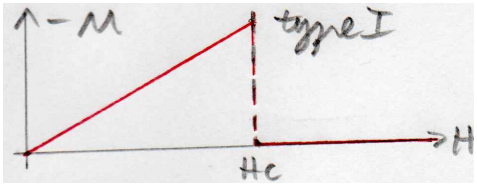

b) 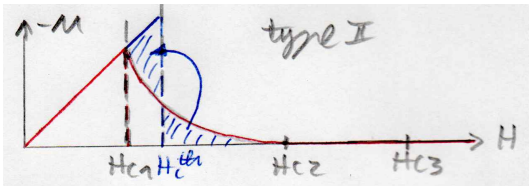

Figure 6.1: Magnetization curves for a) type I and b) type II superconductors.

superconductor

$$E_{\mathrm{mag}}^{\mathrm{II}} = -\mu_0 V \int_0^{H_{c2}} dH\, M(H)\,, \tag{6.1}$$

which corresponds to the area below the magnetization curve, and identifies it with the magnetization energy of a fictitious type I superconductor

$$E_{\mathrm{mag}}^{\mathrm{I}} = \frac{\mu_0}{2} V H_{\mathrm{c}}^{\mathrm{th}\,2}\,. \tag{6.2}$$

This yields a condition defining the thermodynamic critical field H_c^{th}:

$$-\int_0^{H_{c2}} dH\, M(H) = \frac{1}{2}\, H_{\mathrm{c}}^{\mathrm{th}\,2}\,. \tag{6.3}$$

Note a similar energetic consideration was performed for type I superconductors in (2.39) in order to describe their intermediate state. In the following we apply different concepts in order to determine the critical magnetic fields within the realm of the Ginzburg-Landau theory:

1. The upper critical field H_{c2} represents a volume field strength, where the superconducting order parameter starts to become non-zero. Therefore, it will turn out that H_{c2} follows from linearizing the Ginzburg-Landau equations and from solving the corresponding eigenvalue problem.

2. Instead, the lower critical field H_{c1} follows from thermodynamic considerations. To this end one equates the free enthalpies of both the Meissner and the Shubnikov phase

   $$G_{\mathrm{Meissner}}(H_{\mathrm{c1}}) = G_{\mathrm{Shubnikov}}(H_{\mathrm{c1}}) \tag{6.4}$$

   and determines from that condition H_{c1}.

6.2 Upper Critical Field

The state of a superconductor is described by the yields ψ^*, ψ, $\mathbf{A}$ and $\mathbf{j}_{\mathrm{s}}$. According to the Ginzburg-Landau theory they are coupled by the equations (5.46), (5.56) and (5.59):

$$\frac{1}{2m_{\mathrm{s}}}\left(-i\hbar\boldsymbol{\nabla} - e_{\mathrm{s}}\mathbf{A}\right)^2\psi = -\alpha\psi - \beta|\psi|^2\psi\,, \tag{6.5}$$

$$\mathbf{j}_{\mathrm{s}} = \frac{i\hbar e_{\mathrm{s}}}{2m_{\mathrm{s}}}\left(\psi\boldsymbol{\nabla}\psi^* - \psi^*\boldsymbol{\nabla}\psi\right) - \frac{e_{\mathrm{s}}^2}{m_{\mathrm{s}}}\mathbf{A}|\psi|^2\,, \tag{6.6}$$

$$\mathrm{rot}\,\mathbf{B} = \mu_0\,\mathbf{j}_{\mathrm{s}}\,. \tag{6.7}$$

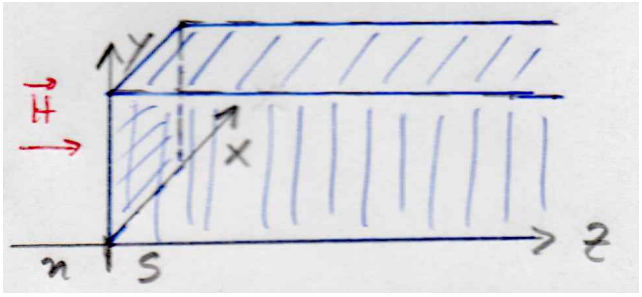

Figure 6.2: Geometry for determining the upper critical field H_{c2}.

Thus, the question arises which assumptions allow to determine the upper critical field H_{c2} from these coupled equations. To this end, we have to specify in particular the underlying geometry.

6.2.1 Assumptions

To be specific, let us choose as a geometry the Fig. 6.2. The xy-plane separates the right half space of the superconductor from the left half space of the normal conductor or the vacuum. The external magnetic field $\mathbf{H}$ is supposed to be pointing in z-direction, so it is perpendicular to the ns-interface. This geometry allows now for the following simplifications to determine the upper critical field H_{c2}.

Coming from higher magnetic fields we investigate the transition point H_{c2}, where the superconductor just starts to turn from the normal conducting into the superconducting state. Thus, only few superconducting electrons exist and the order parameter ψ is small in comparison to the bulk equilibrium value ψ_0, i.e. we have

$$\psi \ll \psi_0 \,. \tag{6.8}$$

The smallness condition (6.8) allows to linearize the Ginzburg-Landau equations (6.5)–(6.7) with respect to the order parameter ψ. At first, we obtain due to the linearization in ψ from (6.6) that there are no superconducting currents in the bulk:

$$\mathbf{j}_s(\mathbf{r}) = \mathbf{0} \,. \tag{6.9}$$

According to (6.7) this has the consequence that the magnetic induction $\mathbf{B}$ turns out to be spatially homogeneous in the bulk and is given by the external magnetic field:

$$\mathbf{B}(\mathbf{r}) = \mu_0 \mathbf{H}(\mathbf{r}) = \mu_0 H_z \mathbf{e}_z = B_z \mathbf{e}_z \,. \tag{6.10}$$

A vector potential $\mathbf{A}(\mathbf{r})$, which respects the Coulomb gauge (4.149), and corresponds to the magnetic induction (6.10) due to (4.31) is given by

$$\mathbf{A}(\mathbf{r}) = B_z \begin{pmatrix} 0 \\ x \\ 0 \end{pmatrix} \,. \tag{6.11}$$

Indeed, with this we get

$$\mathrm{rot}\,\mathbf{A}(\mathbf{r}) = \begin{vmatrix} \mathbf{e}_x & \mathbf{e}_y & \mathbf{e}_z \\ \dfrac{\partial}{\partial x} & \dfrac{\partial}{\partial y} & \dfrac{\partial}{\partial z} \\ 0 & B_z x & 0 \end{vmatrix} = B_z \begin{pmatrix} 0 \\ 0 \\ 1 \end{pmatrix}, \tag{6.12}$$

which corresponds to (6.10). And, finally, a linearization of the Ginzburg-Landau equation (6.6) with respect to ψ yields the equation

$$\frac{1}{2m_\mathrm{s}} \left(-i\hbar\boldsymbol{\nabla} - e_\mathrm{s}\mathbf{A}\right)^2 \psi = -\alpha\psi\,, \tag{6.13}$$

which represents an eigenvalue problem. In the next subsection we physically identify this eigenvalue problem and solve it.

6.2.2 Eigenvalue Problem

Multiplying out the brackets in (6.12) yields

$$-\frac{\hbar^2}{2m_\mathrm{s}}\Delta\psi + \frac{i\hbar e_\mathrm{s}}{m_\mathrm{s}}\mathbf{A}\cdot\boldsymbol{\nabla}\psi + \frac{i\hbar e_\mathrm{s}}{2m_\mathrm{s}}(\boldsymbol{\nabla}\cdot\mathbf{A}) + \frac{e_\mathrm{s}^2}{2m_\mathrm{s}}\mathbf{A}^2\psi = -\alpha\psi\,. \tag{6.14}$$

Inserting therein the vector potential (6.11) we get

$$-\frac{\hbar^2}{2m_\mathrm{s}}\Delta\psi + \frac{i\hbar e_\mathrm{s}}{m_\mathrm{s}}B_z\,x\frac{\partial\psi}{\partial y} + \frac{e_\mathrm{s}^2}{2m_\mathrm{s}}B_z^2\,x^2\psi = -\alpha\psi\,. \tag{6.15}$$

Here it is reasonable to perform the separation ansatz

$$\psi(x,y,z) = e^{i(\gamma\,y+\delta\,z)}\varphi(x)\,, \tag{6.16}$$

which effectively reduces the three-dimensional problem to a one-dimensional one:

$$-\frac{\hbar^2}{2m_\mathrm{s}}\frac{d^2\varphi(x)}{dx^2} - \frac{\hbar e_\mathrm{s}}{m_\mathrm{s}}B_z\,\gamma\,x\,\varphi(x) + \frac{e_\mathrm{s}^2}{2m_\mathrm{s}}B_z^2\,x^2\varphi(x) = -\left[\alpha + \frac{\hbar^2}{2m_\mathrm{s}}(\gamma^2+\delta^2)\right]. \tag{6.17}$$

A quadratic completion allows to convert (6.17) to the standard form of a Schrödinger equation for a one-dimensional harmonic oscillator:

$$\frac{e_\mathrm{s}^2B_z^2}{2m_\mathrm{s}}x^2 - \frac{\hbar e_\mathrm{s}}{m_\mathrm{s}}B_z\,\gamma\,x = \frac{e_\mathrm{s}^2B_z^2}{2m_\mathrm{s}}\left(x - \frac{\hbar\gamma}{e_\mathrm{s}B_z}\right)^2 - \frac{\hbar^2\gamma^2}{2m_\mathrm{s}}\,. \tag{6.18}$$

Indeed, due to (6.18) equation (6.17) can be recast into

$$-\frac{\hbar^2}{2m_\mathrm{s}}\frac{d^2\varphi(x)}{dx^2} + \frac{e_\mathrm{s}^2B_z^2}{2m_\mathrm{s}}\left(x - \frac{\hbar\gamma}{e_\mathrm{s}B_z}\right)^2\varphi(x) = -\left(\alpha + \frac{\hbar^2\delta^2}{2m_\mathrm{s}}\right). \tag{6.19}$$

This form suggests to perform the translation

$$x' = x - \frac{\hbar\gamma}{e_\mathrm{s}B_z} \tag{6.20}$$

to introduce the cyclotron frequency

$$\omega_0 = \frac{e_\mathrm{s} B_z}{m_\mathrm{s}} \tag{6.21}$$

and to redefine

$$\alpha' = \alpha + \frac{\hbar^2 \delta^2}{2m_\mathrm{s}} \,. \tag{6.22}$$

Indeed, with applying (6.20)–(6.22), we can convert (6.19) into the standard Schrödinger equation for a one-dimensional harmonic oscillator:

$$\left(-\frac{\hbar^2}{2m_\mathrm{s}} \frac{d^2}{dx'^2} + \frac{1}{2} m_\mathrm{s} \omega_0^2 x'^2 \right) \varphi(x') = -\alpha' \varphi(x') \,. \tag{6.23}$$

Due to quantum mechanics we obtain immediately the solutions of this eigenvalue problem. The eigenvalues read

$$-\alpha'_n = \hbar\omega_0 \left(n + \frac{1}{2} \right) \tag{6.24}$$

and the eigenfunctions are given by

$$\varphi_n(x') = N_n H_n \left(\sqrt{\frac{m_\mathrm{s}\omega_0}{\hbar}} x' \right) e^{-m_\mathrm{s}\omega_0 x'^2/2\hbar} \,. \tag{6.25}$$

6.2.3 Quantum Mechanics

In quantum mechanics the motion of a charged particle in a homogeneous magnetic field is described by the eigenvalue problem (6.23). The allowed energy levels follow from (6.21) and (6.24):

$$E_n = -\alpha'_n = \hbar\omega_0 \left(n + \frac{1}{2} \right) + \frac{\hbar^2 \delta^2}{2m_\mathrm{s}} \,. \tag{6.26}$$

The second term corresponds to the kinetic energy of the translational motion in z-direction, whereas the first term describes the energy of the motion in the plane perpendicular to it. Note that the latter energy can be recast by taking into account (6.21) into the potential energy of a magnetic moment in the magnetic field (6.10):

$$E_n = -\mathbf{m}_n \cdot \mathbf{B} + \frac{\hbar^2 \delta^2}{2m_\mathrm{s}} \,, \qquad m_{zn} = m_\mathrm{B}(2n+1) \,. \tag{6.27}$$

Here the Bohr magneton

$$m_\mathrm{B} = -\frac{\hbar e_\mathrm{s}}{2m_\mathrm{s}} \tag{6.28}$$

appears, which represents the unit of the magnetic moment of the charge $-e_\mathrm{s}$ and the mass m_s. Furthermore, the eigenfunctions (6.25) correspond to the classical circular motion of a charged particle in the xy-plane, which is perpendicular to the direction of the magnetic field, see Fig. 6.3a). But the allowed energy levels are discrete Landau levels

$$\frac{\hbar^2}{2m_\mathrm{s}} \left(k_x^2 + k_y^2 \right) = \hbar\omega_0 \left(n + \frac{1}{2} \right) \,, \tag{6.29}$$

which yield discrete Landau cylinders within the Fermi sphere, see Fig. 6.3b).

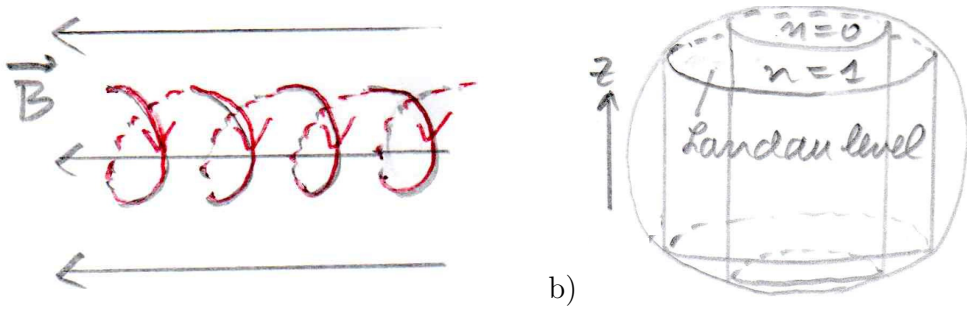

a) b)

Figure 6.3: a) Classical cirular motion of charge $-e_\mathrm{s}$ around magnetic field (6.10) with cyclotron frequency (6.21). b) Quantized Landau cylinders with discrete Landau levels (6.28) within the Fermi sphere.

6.2.4 Upper Critical Field

In quantum mechanics the magnetic field is applied from outside, which is therefore given. And one determines from the quantum mechanical eigenvalue problem the allowed Landau levels as the energy eigenvalues. But in the Ginzburg-Landau theory of a superconductor the inverse problem occurs. Here the eigenvalue α represents a Landau coefficient, whose temperature dependence is a phenomenologically given according to (5.10). Thus, conversely, we are aiming here for the largest possible magnetic field as this corresponds to the upper critical field $B_{\mathrm{c}2}$.

To this end we use (6.20), (6.21), and (6.23) and solve for the magnetic field:

$$B_z(n,\delta) = \frac{2m_s}{\hbar e_s}\left(-\alpha - \frac{\hbar^2\delta^2}{2m_s}\right)\frac{1}{2n+1}\,. \tag{6.30}$$

Note that for $T < T_\mathrm{c}$ we have $\alpha < 0$ due to (5.10). We read off from (6.30) that the magnetic field $B_z(n,\delta)$ is largest for the quantum numbers $n = 0$ and $\delta = 0$:

$$B_{\mathrm{c}2} = \max_{\substack{n\in\mathbb{N}\\ \delta\in\mathbb{R}}} B_z(n,\delta) = B_z(0,0) = \frac{-2m_\mathrm{s}\alpha}{\hbar e_\mathrm{s}}\,. \tag{6.31}$$

All other magnetic fields $B_z(n,\delta)$ for $n \neq 0$ and $\delta \neq 0$ do not have any physical meaning as the approximation (6.8) would no larger hold.

6.2.5 Consequences

We can now relate the upper critical field (6.31) to the thermodynamic critical field B_c^th. The latter follows from identifying the magnetic field energy (6.2) with the condensation energy (5.17) of the Landau theory:

$$\frac{\alpha^2}{2\beta} = \frac{B_\mathrm{c}^{\mathrm{th}\,2}}{2\mu_0} \qquad \Longrightarrow \qquad B_\mathrm{c}^\mathrm{th} = \frac{-\mu_0\alpha}{\beta}\,. \tag{6.32}$$

material	T_c	κ
Nb_3Sn	18 K	30
$YBa_2Cu_3O_7$	93 K	100

Table 6.1: Critical temperature T_c and Ginzburg-Landau parameter κ for some superconductors of type II.

The ratio of the magnetic fields (6.31) and (6.32) turns out to be temperature independent due to (5.11):

$$\frac{B_{c2}}{B_c^{th}} = \frac{2m_s}{\hbar e_s}\sqrt{\frac{\beta}{\mu_0}}\,. \tag{6.33}$$

In order to interpret (6.33) physically, we have to recall that the Ginzburg-Landau theory is characterized by two length scales, namely the Landau penetration length following from (5.24) and (5.64)

$$\lambda_L = \sqrt{\frac{m_s\beta}{e_s^2\mu_0\alpha_c'(T_c - T)}} \sim \frac{1}{\sqrt{T_c - T}} \tag{6.34}$$

and the coherence length following from (5.10) and (5.69)

$$\xi = \sqrt{\frac{\hbar^2}{2m_s(T_c - T)\alpha_c'}} \sim \frac{1}{\sqrt{T_c - T}}\,, \tag{6.35}$$

whose ratio (5.4) yields the temperature independent Ginzburg-Landau parameter

$$\kappa = \frac{\lambda_L}{\xi} = \frac{m_s}{\hbar e_s}\sqrt{\frac{2\beta}{\mu_0}}\,. \tag{6.36}$$

Thus, the ratio of the magnetic fields (6.33) is given by the Ginzburg-Landau parameter:

$$\frac{B_{c2}}{B_c^{th}} = \sqrt{2}\kappa \qquad \Longrightarrow \qquad B_{c2} = \sqrt{2}\kappa B_c^{th}\,. \tag{6.37}$$

6.2.6 Discussions

1. Some exemplary values for Ginzburg-Landau parameters in Fig. 6.1 show that superconductors of type II have, due to (6.37), the generic property

$$B_{c2} \gg B_c^{th}\,, \tag{6.38}$$

see also Fig. 6.1b).

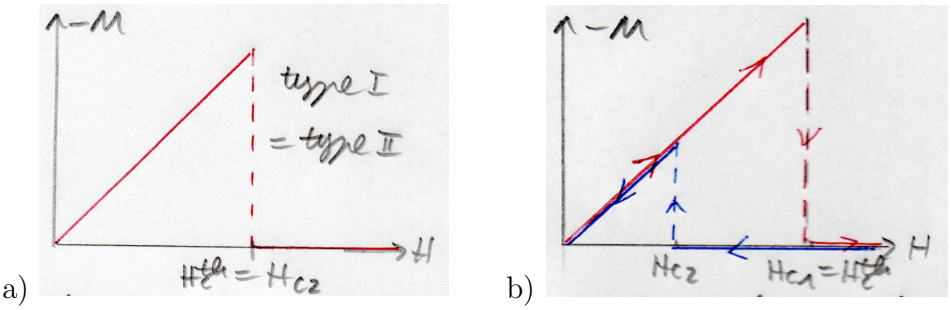

a) b)

Figure 6.4: Magnetization curves for a) $\kappa_c = 1/\sqrt{2}$ and b) $\kappa < \kappa_c = 1/\sqrt{2}$.

2. From (6.37) we also read off that the limiting case $\kappa_c = 1/\sqrt{2}$ yields $B_{c2} = B_c^{th}$. Thus, in that case the magnetization curves of type II and type I superconductors turn out to coincide, see Fig. 6.4a).

3. Which physical meaning has the case $H_{c2} < H_c^{th}$ for superconductors of type I, which are characterized by $\kappa < \kappa_c = 1/\sqrt{2}$? Here one observes a hysteresis effect as is depicted in Fig. 6.4b). Coming from higher magnetic fields the Meissner phase starts at $H_{c2} < H_c^{th}$, whereas coming from lower magnetic fields the Meissner phase ends at $H_{c1} = H_c^{th}$. Measuring the hysteresis, i.e. the two magnetic fields H_{c2} and H_c^{th}, allows to determine due to (6.37) the upper boundary of the Ginzburg-Landau parameter, i.e. $\kappa_c = 1/\sqrt{2} \approx 0.7$. For instance, for pure aluminium one gets $\kappa = 0.03$ and for pure indium we have $\kappa = 0.06$.

   Note that a similar hysteresis effect is well known at the first-order phase transition from liquid to solid water and is called there hypothermia, i.e. Unterkühlung in German. This hysteresis effect therefore underlines the previous statement that the transition from a normal to a superconducting phase at non-vanishing magnetic field is of first order.

4. According to (5.10) the upper critical field (6.33) has the temperature dependence

$$B_{c2} \sim (T_c - T)^\gamma \tag{6.39}$$

   with the mean-field exponent $\gamma_{MF} = 1$. Instead, experiments yield the value $\gamma \approx 0.64$. This discrepancy can be explained by huge thermal fluctuations, which are present in the vicinity of the critical point T_c.

5. From the magnetic flux quantum (4.97) and the coherence length (6.35) we conclude by taking into account (5.10) and (6.31)

$$\frac{\phi_0}{2\pi\xi^2} = \frac{2\pi\hbar}{e_s}\frac{2m_s(T_c - T)\alpha_c'}{2\pi\hbar^2} = \frac{-2m_s\alpha}{\hbar e_s} = B_{c2}\,. \tag{6.40}$$

   Thus, at the upper critical field B_{c2} one single flux quantum ϕ_0 is frozen in the area $2\pi\xi^2$.

6. Combining (6.37) and (6.39) with (6.4) we conclude for the thermodynamic critical field

$$B_c^{th} = \frac{B_{c2}}{\sqrt{2}\kappa} = \frac{\phi_0}{\sqrt{2}2\pi\xi^2\kappa} = \frac{\phi_0}{2\sqrt{2}\pi\lambda_L\xi}\,. \tag{6.41}$$

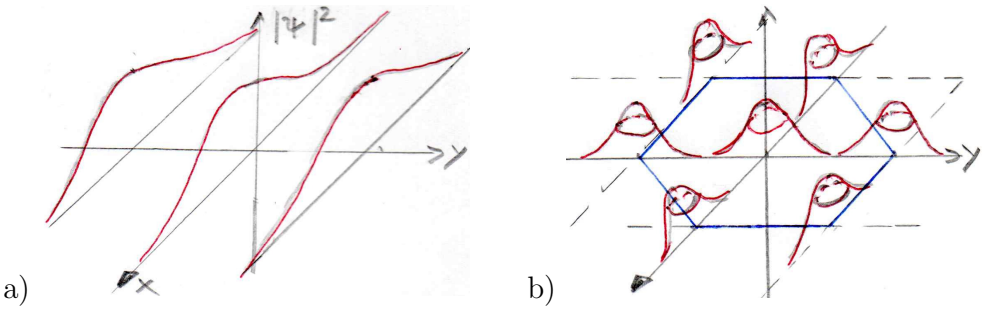

Figure 6.5: Superconducting density: a) according to (6.16) and (6.25) for $n = 0$ as well as b) due to a suitable superposition (6.45).

Thus, $B_{\mathrm{c}}^{\mathrm{th}}$ corresponds to a flux quantum ϕ_0 being frozen in the area $2\sqrt{2}\pi\lambda_{\mathrm{L}}\xi$.

6.2.7 Flux Line Lattice

At the upper critical field (6.31) only the eigenfunction (6.24) with $n = 0$ appears. It represents a Gauß function with a width, which is given by the oscillator length

$$l_{\mathrm{osc}} = \sqrt{\frac{\hbar}{m_{\mathrm{s}}\omega_0}}\,. \tag{6.42}$$

Taking into account the cyclotron frequency (6.20), the oscillator length (6.42) turns out to be independent of the mass m_{s}:

$$l_{\mathrm{osc}} = \sqrt{\frac{\hbar}{e_{\mathrm{s}}B_z}}\,. \tag{6.43}$$

Thus, decreasing the magnetic field $B_z > B_{\mathrm{c},2}$ yields an increasing oscillator length (6.43), until at the upper critical magnetic field (6.31) the oscillator length coincides with the coherence length (6.35):

$$l_{\mathrm{osc}} = \sqrt{\frac{\hbar^2}{2m_{\mathrm{s}}(T_{\mathrm{c}} - T)\alpha_{\mathrm{c}}'}} = \xi\,. \tag{6.44}$$

Furthermore, we note that the eigenfunctions following from (6.16) and (6.25) for $n = 0$ do not yield any density modulation in y-direction, see Fig. 6.5a). Therefore, they are not suitable to describe a flux line lattice, which is supposed to exist in the Shubnikov phase. But in the separation ansatz (6.16), where we have to set $\delta = 0$ due to the upper critical field (6.31), we still have a degeneracy with respect to γ. Thus, combining (6.16), (6.20), (6.25), and (6.44) the general solution at the upper critical magnetic field $B_{\mathrm{c},2}$ is given by the superposition

$$\psi(x, y, z) = \int d\gamma\, c(\gamma) \exp\left\{ i\gamma y - \frac{1}{2\xi^2}\left(x - \frac{\hbar\gamma}{esB_{\mathrm{c}2}}\right)^2 \right\}. \tag{6.45}$$

a) 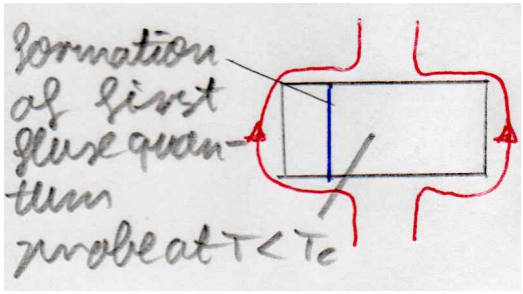

b) 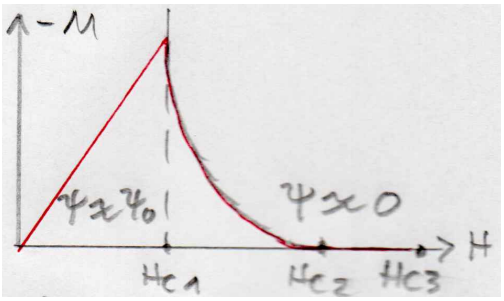

Figure 6.6: a) The formation of the first flux quantum implies that b) the Meissner-Ochselfeld effect is reduced.

A suitable choice of $c(\gamma)$ yields now a modulation of the order parameter in the xy-plane. Candidates for a two-dimensional flux line lattice are a square and a hexagonal lattice. the former was predicted by Abrikosov, but the experiment showed that the latter is realised in the Shubnikov phase, see Fig. 6.5b).

6.3 Lower Critical Field

The lower critical field H_{c1} is characterised by the formation of the first flux quantum as is illustrated in Fig. 6.6a). As the core of the flux quantum is normal conducting this consequently leads to a reduction of the Meissner-Ochselfeld effect, see Fig. 6.6b).

The transition from the Meissner phase $0 \leq H \leq H_{c1}$, where no flux quanta exist, to the Shubnikov phase $H_{c1} \leq H \leq H_{c2}$ where flux quanta do exist, can be described as a phase transition of first order from the point of view of thermodynamics. The lower critical field H_{c1} turns out to result from equating the respective free enthalpies for both phases according to (6.4). Whereas G_{Meissner} is lower than $G_{\text{Shubnikov}}$ for $0 \leq H \leq H_{c1}$, conversely, $G_{\text{Shubnikov}}$ is lower than G_{Meissner} for $H_{c1} \leq H \leq H_{c2}$, see Fig. 6.7. At the lower critical field $H = H_{c1}$ both free enthalpies coincide, so (6.4) determines H_{c1}.

6.3.1 Starting Point

We assume the superconductor to be so large, that surface effects are negligible. This means, in particular, that surface terms can be neglected when the free enthalpies in both the Meissner and the Shubnikov phase are evaluated. According to the Ginzburg-Landau theory the full expresion for the free enthalpy is given by (5.40).

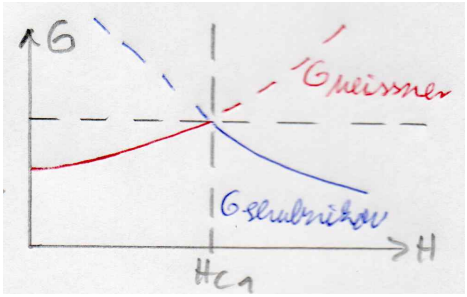

Figure 6.7: Free enthalpies of a superconductor below H_{c1} in the Meissner phase and above H_{c1} in the Shubnikov phase.

6.3.2 Meissner Phase

In the Meissner phase a flux quantum has not yet emerged. Thus, spatial inhomogeneities of the order parameter ψ can only occur at the surface of the superconductor. But such surface contributions can be neglected according to the previous subsection. Therefore, we specialize (5.40) in the Meissner phase by demanding

$$\psi = \psi_0\,, \qquad \boldsymbol{\nabla}\psi = \boldsymbol{\nabla}\psi^* = \mathbf{0}\,. \tag{6.46}$$

Furthermore, we know that the Meissner-Ochsenfeld effect is present in the Meissner phase, so we have also

$$\mathbf{B} = \mathbf{A} = \mathbf{0}\,. \tag{6.47}$$

Inserting (6.46) and (6.46) in (5.40) we obtain for the free enthalpy of the Meissner phase:

$$G_{\text{Meissner}} = G_{\text{n}} + \int_V dV \left\{ \alpha|\psi_0|^2 + \frac{\beta}{2}|\psi_0|^4 + \frac{\mu_0}{2}\,\mathbf{H}^2 \right\}. \tag{6.48}$$

6.3.3 Shubnikov Phase

In the Shubnikov phase we cannot make any simplifying assumption as, for instance, (6.46) and (6.47). When one flux quantum exists, the order parameter changes there spatially and also the Meissner-Ochsenfeld effect breaks down. Thus, in the Shubnikov phase the full expression of the free enthalpy (5.40) has to be taken into account.

6.3.4 Free Enthalpy Balance

Inserting (5.40) for the Shubnikov phase and (6.48) for the Meissner phase into (6.4) we obtain the following equilibrium condition for determining the lower critical field:

$$\int dV \left[\alpha \left(|\psi|^2 - |\psi_0|^2 \right) + \frac{\beta}{2} \left(|\psi|^4 - |\psi_0|^4 \right) + \frac{1}{2m_{\text{s}}} | - i\hbar\boldsymbol{\nabla}\psi - e_{\text{s}}\mathbf{A}\psi|^2 + \frac{\mathbf{B}^2}{2\mu_0} \right] = \int dV\, \mathbf{B}\cdot\mathbf{H}_{\text{c1}}$$

Both the left- and the right-hand side allow for a concrete physical interpretation:

1. The left-hand side is only non-vanishing in the vicinity of a flux line. Assuming a cylinder symmetry for the flux quantum, the volume integral can be decomposed as follows

$$dV = L\, dF\,. \tag{6.49}$$

With this we obtain the line energy ε_L with the physical dimension $[\varepsilon_\mathrm{L}] = 1\,\mathrm{J/m}$, which is needed for generating the flux quantum:

$$\varepsilon_\mathrm{L} = \int dF \left[\alpha\left(|\psi|^2 - |\psi_0|^2\right) + \frac{\beta}{2}\left(|\psi|^4 - |\psi_0|^4\right) + \frac{1}{2m_\mathrm{s}}|-i\hbar\boldsymbol{\nabla}\psi - e_\mathrm{s}\mathbf{A}\psi|^2 + \frac{\mathbf{B}^2}{2\mu_0}\right]. \tag{6.50}$$

2. The right-hand side represents the interaction of the flux quantum with the magnetic field. It corresponds to the energy, which is released due to the generation of the flux quantum. Applying the decomposition (6.49) also to the right-hand side, the equilibrium condition is rewritten as

$$\varepsilon_\mathrm{L} = H_\mathrm{c1}\int_F B dF\,. \tag{6.51}$$

In case that only one single flux quantum is present, the area integral in (6.51) yields the flux quantum ϕ_0

$$\int_F B\cdot dF = \phi_0\,, \tag{6.52}$$

so the lower critical field H_c1 is given by

$$H_\mathrm{c1} = \frac{\varepsilon_\mathrm{L}}{\phi_0}\,. \tag{6.53}$$

Thus, the calculation of the lower critical field H_c1 is traced back to determining the line energy (6.50).

6.3.5 Splitting of Line Energy

For practical purposes we split the line energy (6.50) for a single flux quantum into two pieces:

$$\varepsilon_\mathrm{L} = \varepsilon_\mathrm{L}^\psi + \varepsilon_\mathrm{L}^B\,. \tag{6.54}$$

The first piece $\varepsilon_\mathrm{L}^\psi$ depends on the order parameter ψ, whereas the second piece ε_L^B is governed by the magnetic field. Note that the interaction energy $-\mathbf{j}_\mathrm{s}\cdot\mathbf{A}$ from (5.35) between the superconducting current density $\mathbf{j}_\mathrm{s}$ and the vector potential $\mathbf{A}$ is partially counted for $\varepsilon_\mathrm{L}^\psi$ and ε_L^B, respectively, due to (5.59):

$$\varepsilon_\mathrm{L}^\psi = \int dF \left[\alpha\left(|\psi|^2 - |\psi_0|^2\right) + \frac{\beta}{2}\left(|\psi|^4 - |\psi_0|^4\right) + \frac{\hbar^2}{2m_\mathrm{s}}|\boldsymbol{\nabla}\psi|^2 - \frac{i\hbar e_\mathrm{s}}{2m_\mathrm{s}}\left(\psi\boldsymbol{\nabla}\psi^* - \psi^*\boldsymbol{\nabla}\psi\right)\right], \tag{6.55}$$

$$\varepsilon_\mathrm{L}^B = \int dF \left(\frac{\mathbf{B}^2}{2\mu_0} + \frac{e_\mathrm{s}^2}{2m_\mathrm{s}}\mathbf{A}^2|\psi|^2\right). \tag{6.56}$$

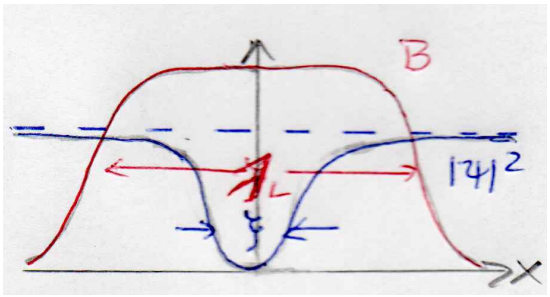

Figure 6.8: For type II superconductors spatial profiles of magnetic induction B and superconducting electron density $|\psi|^2$ near a flux quantum vary on the scales of the London penetration length λ_{L} and the coherence length ξ, respectively, following (6.57).

An exact calculation of the line energy (6.54)–(6.56) would assume to know the precise spatial shape of both the order parameter ψ and the vector potential $\mathbf{A}$ in the vicinity of the flux quantum. To this end one would have to solve for this situation the corresponding Ginzburg-Landau equations. As this is not possible, we reside here to a specific approximation.

6.3.6 Approximation

In the following we proceed with calculating the line energy (6.54)–(6.56) for the case

$$\kappa = \frac{\lambda_{\mathrm{L}}}{\xi} \gg 1\,, \tag{6.57}$$

i.e. for extreme type II superconductors. This is insofar reasonable as the Shubnikov phase only exists for type II superconductors. For instance, the assumption (6.57) is well justified for high T_{c}-superconductors, where we have about $\kappa = 100$. And, finally, we note that (6.57) corresponds to the situation that the Ginzburg-Landau theory goes over into the Landau theory as was already discussed in subsection 5.4.1. Thus, in the following we only have to find an efficient way how to implement the approximation (6.57) into the concrete calculation.

6.3.7 Calculation of First Line Energy

Furthermore, although subsection 5.4.2 dealt with the case opposite to (6.57), i.e. $\lambda_{\mathrm{L}} \ll \xi$, we can still use here the generic result that the order parameter varies linearly in the center of the flux quantum, see Fig. 6.8. Thus, we perform the ansatz in cylinder coordinates

$$\psi(r) = \psi_0 \frac{r}{\xi} e^{i\varphi}\,, \qquad \psi_0^2 = -\frac{\alpha}{\beta}\,, \qquad 0 \leq r \leq \xi\,. \tag{6.58}$$

Due to this ansatz (6.58) the gradient terms of the order parameter in (6.55) representing the first current term in (6.55) vanishes, which is in accordance with the corresponding discussion subsection 5.4.1. Thus, we have only a contribution stemming from ψ

$$\varepsilon_{\mathrm{L},1}^{\psi} = \int dF \left[\alpha\left(|\psi|^2 - |\psi_0|^2\right) + \frac{\beta}{2}\left(|\psi|^4 - |\psi_0|^4\right)\right] \tag{6.59}$$

and another one depending on the gradient of ψ

$$\varepsilon_{\mathrm{L},2}^{\psi} = \int dF \, \frac{\hbar^2}{2m_{\mathrm{s}}} |\boldsymbol{\nabla}\psi|^2 \,. \tag{6.60}$$

Inserting (6.58) in (6.59) yields

$$\varepsilon_{\mathrm{L},1}^{\psi} = \int dF \left[\alpha - \frac{\alpha}{\beta}\left(\frac{r^2}{\xi^2} - 1\right) + \frac{\alpha^2}{2\beta}\left(\frac{r^4}{\xi^4} - 1\right)\right] = \int dF \, \frac{\alpha^2}{2\beta}\left(1 - \frac{2r^2}{\xi^2} + \frac{r^4}{\xi^4}\right) . \tag{6.61}$$

Taking into account (6.32), i.e. the condensation energy expressed in terms of the thermodynamic initial field $B_{\mathrm{c}}^{\mathrm{th}}$, and evaluating (6.61) further with polar coordinates, we get

$$\varepsilon_{\mathrm{L},1}^{\psi} = \frac{B_{\mathrm{c}}^{\mathrm{th}\,2}}{2\mu_0} 2\pi \int_0^{\xi} dr \left(r - \frac{2r^3}{\xi^2} + \frac{r^5}{\xi^4}\right) = \frac{B_{\mathrm{c}}^{\mathrm{th}\,2}}{2\mu_0} \frac{\pi\xi^2}{3} \,. \tag{6.62}$$

Here the first factor represents an energy per volume and the second factor coincides with 1/3 of the area of a flux quantum. Expressing the thermodynamic critical field $B_{\mathrm{c}}^{\mathrm{th}}$ by the flux quantum ϕ_0 according to (6.40) we can convert (6.62) into the form

$$\varepsilon_{\mathrm{L},1}^{\psi} = \frac{\pi}{12\mu_0}\left(\frac{\phi_0}{2\pi\lambda_{\mathrm{L}}}\right)^2 . \tag{6.63}$$

Now we turn out attention to (6.60) and argue, why we have to take it into account within the ansatz (6.58). To this end we note

$$\frac{\partial}{\partial x}\sqrt{x^2+y^2} = \frac{x}{\sqrt{x^2+y^2}} \qquad \Longrightarrow \qquad |\boldsymbol{\nabla}\psi| = \frac{\psi_0}{\xi} \,. \tag{6.64}$$

Thus, inserting (6.58) in (6.60) as well as taking into account (5.69), (6.32), and (6.40) yields

$$\varepsilon_{\mathrm{L},2}^{\psi} = \int dF \, \frac{-\hbar^2\alpha}{2m_s\beta\xi^2} = \frac{\alpha^2}{2\beta}\left(-\frac{\hbar^2}{2m_s\alpha\xi^2}\right) 2\pi\xi^2 = \frac{B_{\mathrm{c}}^{\mathrm{th}\,2}}{2\mu_0} 2\pi\xi^2 = \frac{\pi}{2\mu_0}\left(\frac{\phi}{2\pi\lambda_L}\right)^2 . \tag{6.65}$$

We conclude that (6.65) turns out to be even larger than (6.63). Thus, (6.65) can not be neglected.

6.3.8 Calculation of Second Line Energy

The line energy (6.55) contains two contributions. The first one represents the magnetic energy. And taking into account (5.36), (5.37) the second contribution in (6.55) corresponds to the kinetic energy of the superconducting electrons in the London theory. Applying (4.16), (4.33) and (M2), i.e. $\operatorname{rot}\mathbf{B} = \mu_0\mathbf{j}_{\mathrm{s}}$ in the stationary case, we obtain from (6.55)

$$\varepsilon_{\mathrm{L}}^{B} = \int dF \left[\frac{\mathbf{B}^2}{2\mu_0} + \frac{e_{\mathrm{s}}^2 n_{\mathrm{s}}}{2m_{\mathrm{s}}}\left(\frac{m_{\mathrm{s}}}{e_{\mathrm{s}}^2 n_{\mathrm{s}}}\right)^2 \frac{1}{\mu_0^2} (\operatorname{rot}\mathbf{B})^2\right] , \tag{6.66}$$

which reduces with the London penetration length (4.51) to

$$\varepsilon_{\mathrm{L}}^{B} = \frac{1}{2\mu_0}\int dF \left[\mathbf{B}^2 + \lambda_{\mathrm{L}}^2 (\operatorname{rot}\mathbf{B})^2\right] . \tag{6.67}$$

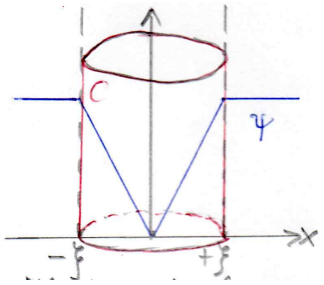

Figure 6.9: Cut-off cylinder C regularizing divergencies near the origin of flux quantum.

In order to further facilitate the evaluation of (6.67) we apply the vector analytic identity (5.54) with $\mathbf{u} = \operatorname{rot}\mathbf{B}$ and $\mathbf{u} = \mathbf{B}$, yielding

$$\varepsilon_{\mathrm{L}}^{B} = \frac{1}{2\mu_0}\int dF\,\Big[\mathbf{B}^2 + \lambda_{\mathrm{L}}^2\,\mathbf{B}\cdot\operatorname{rot}(\operatorname{rot}\mathbf{B}) - \lambda_{\mathrm{L}}^2\operatorname{div}(\operatorname{rot}\mathbf{B}\times\mathbf{B})\Big]\,. \tag{6.68}$$

Applying (6.49) as well as (4.43), (M4), and the Gauss theorem, we decompose (6.68) into a volume and a surface integral:

$$L\,\varepsilon_{\mathrm{L}}^{B} = \frac{1}{2\mu_0}\int_V dV\,\mathbf{B}\cdot\big(\mathbf{B} - \lambda_{\mathrm{L}}^2\,\Delta\mathbf{B}\big) + \frac{\lambda_{\mathrm{L}}^2}{2\mu_0}\oint_{\partial V}(\mathbf{B}\times\operatorname{rot}\mathbf{B})\cdot d\mathbf{F}\,. \tag{6.69}$$

In Section 4.8 we already determined the spatial profile of the magnetic field in the vicinity of the flux quantum in the realm of the London theory. According to (4.144) the magnetic induction is given by the modified Bessel function $K_0(r/\lambda_{\mathrm{L}})$, which has a logarithmic divergence at the origin. Therefore, the respective integrals in (6.69) turn out to diverge as well.

Thus, in order to obtain a finite result for (6.69) it is necessary from a mathematical point of view to introduce a cut-off cylinder C as sketched in Fig. 6.9. Performing the integration over the whole $\mathbb{R}^3$ without the cut-off cylinder, i.e. over $V = \mathbb{R}^3 \setminus C$, the divergency at the origin is avoided.

But the choice of this cut-off cylinder C with the cut-off radius ξ in the xy-plane has not only a mathematical background, it can also be justified on physical grounds:

1. Within the London theory the reasoning reads as follows. As the magnetic induction $\mathbf{B}$ diverges in the limit $r \to 0$, there exists a certain radius $r = \xi$ in the xy-plane, where the critical field B_{c} is reached. Thus, the superconductor is then divided in a normal conducting region for $0 \le r \le \xi$ and a superconducting region for $r \ge \xi$, see Fig. 6.10a). But as the energy (6.69) is only supposed to be evaluated in the superconducting region, the cut-off cylinder C has to be excluded from the integration volume.

2. Another argument follows from taking into account the real profile of the magnetic induction. Whereas the magnetic induction of the London theory diverges at the origin, the real magnetic induction, following from numerical calculations, turns out to be finite everywhere, see Fig. 6.10b). Thus, choosing an appropriate cut-off radius $r = \xi$ one may

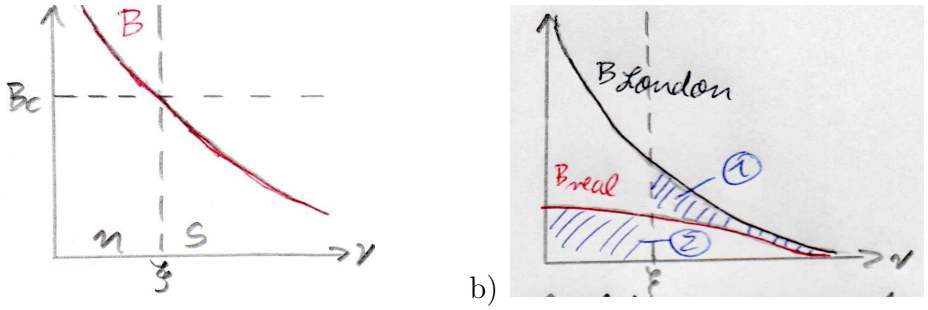

a) b)

Figure 6.10: Vicinity of flux quantum: a) Inner region is normal conducting, whereas outer region is superconducting. b) Although London theory predicts a divergent magnetic induction, a numerical calculation reveals that it remains finite.

achieve that the contribution from ①, which is erroneously included in the London theory, corresponds to the contribution from ②, which is neglected. Therefore, one can even expect to obtain a reasonable quantitative result from introducing the cut-off cylinder C.

At first, we insert the inhomogeneous Helmholtz equation (4.105) into (6.69):

$$L\,\varepsilon_{\mathrm{L}}^{B} = \frac{1}{2\mu_0^2}\int_V dV\,\mathbf{B}\cdot\mathbf{e}_z\,\phi_0\delta^{(2)}(\mathbf{x}) + \frac{\lambda_{\mathrm{L}}^2}{2\mu_0}\oint_{\partial V}(\mathbf{B}\times\operatorname{rot}\mathbf{B})\cdot d\mathbf{F}\,. \tag{6.70}$$

But as the delta function has its singularity at the origin, which is excluded from the integration volume $V = \mathbb{R}^3\backslash C$, the volume integral in (6.70) vanishes and only the surface integral remains. Inserting the Oersted law (5.56) into (6.70) yields

$$L\,\varepsilon_{\mathrm{L}}^{B} = \frac{\lambda_{\mathrm{L}}^2}{2}\oint_{\partial V}(\mathbf{B}\times\operatorname{rot}\mathbf{j}_{\mathrm{s}})\cdot d\mathbf{F}\,. \tag{6.71}$$

From (4.144) and (4.145) we read off $\mathbf{B} = B_z(r)\mathbf{e}_z$ and $\mathbf{j}_{\mathrm{s}} = j_\varphi(r)\mathbf{e}_\varphi$, so taking into account $\mathbf{e}_z\times\mathbf{e}_\varphi = -\mathbf{e}_r$ we obtain

$$L\,\varepsilon_{\mathrm{L}}^{B} = -\frac{\lambda_{\mathrm{L}}^2}{2}\oint_{\partial V}B_z(r)j_\varphi(r)\,\mathbf{e}_r\cdot d\mathbf{F}\,. \tag{6.72}$$

Here the area integral is performed along the surface of the out-off cylinder C, see Fig. 6.9, which is characterized by $d\mathbf{F}\sim -\mathbf{e}_r$:

$$L\,\varepsilon_{\mathrm{L}}^{B} = \frac{\lambda_{\mathrm{L}}^2}{2}\oint_{\partial V}B_z(r)j_\varphi(r)dF\,. \tag{6.73}$$

Integrating over the surface of the cut-off cylinder C, where we have $r=\xi$, the integrand of (6.72) turns out to be constant:

$$L\,\varepsilon_{\mathrm{L}}^{B} = \frac{\lambda_{\mathrm{L}}^2}{2}\,2\pi\xi L B_z(\xi)j_\varphi(\xi) \qquad\Longrightarrow\qquad \varepsilon_{\mathrm{L}}^{B} = \pi\xi\lambda_{\mathrm{L}}^2 B_z(\xi)j_\varphi(\xi)\,. \tag{6.74}$$

Due to (4.144) and (4.145) the modified Bessel functions K_0 and K_1 are evaluated at the argument ξ/λ_{L}, which is small according to the assumption (6.57). Therefore, we approximate (4.144) and (4.145) by the behaviour of the modified Bessel functions K_0, K_1 for small

arguments, see page 59 at the top:

$$L\,\varepsilon_{\mathrm{L}}^{B} = \pi\xi\lambda_{\mathrm{L}}^{2}\,\frac{\phi_0}{2\pi\lambda_{\mathrm{L}}^{2}}\left(\ln\frac{\lambda_{\mathrm{L}}}{\xi}\right)\frac{\phi_0}{\mu_0 2\pi\lambda_{\mathrm{L}}^{3}}\,\frac{\lambda_{\mathrm{L}}}{\xi} \qquad \Longrightarrow \qquad \varepsilon_{\mathrm{L}}^{B} = \frac{\pi}{\mu_0}\left(\frac{\phi_0}{2\pi\lambda_{\mathrm{L}}}\right)^{2}\ln\frac{\lambda_{\mathrm{L}}}{\xi}\,. \tag{6.75}$$

6.3.9 Lower Critical Field

Now we add both contributions (6.63), (6.65) for $\varepsilon_{\mathrm{L}}^{\psi}$ and (6.74) for $\varepsilon_{\mathrm{L}}^{B}$ in order to obtain the total line energy ε_{L} and, finally via (6.53), the lower critical field

$$H_{\mathrm{c1}} = \frac{\pi}{\mu_0\phi_0}\left(\frac{\phi_0}{2\pi\lambda_{\mathrm{L}}}\right)^{2}\left(\ln\frac{\lambda_{\mathrm{L}}}{\xi}+\frac{7}{12}\right)\,. \tag{6.76}$$

Inserting therein the thermodynamic critical field (6.41), we get

$$B_{\mathrm{c1}} = B_{\mathrm{c}}^{\mathrm{th}}\,\frac{2\sqrt{2}\pi\lambda_{\mathrm{L}}\xi}{\phi_0}\,\frac{\pi}{\phi_0}\,\frac{\phi_0^{2}}{4\pi^{2}\lambda_{\mathrm{L}}^{2}}\left(\ln\frac{\lambda_{\mathrm{L}}}{\xi}+\frac{7}{12}\right) = \sqrt{2}B_{\mathrm{c}}^{\mathrm{th}}\,\frac{\xi}{2\lambda_{\mathrm{L}}}\left(\ln\frac{\lambda_{\mathrm{L}}}{\xi}+\frac{7}{12}\right)\,. \tag{6.77}$$

Thus, introducing the Ginzburg-Landau parameter $\kappa = \lambda_{\mathrm{L}}/\xi$ we, finally, obtain

$$B_{\mathrm{c1}}(\kappa) = B_{\mathrm{c}}^{\mathrm{th}}\,\frac{\sqrt{2}}{2\kappa}\left(\ln\kappa+\frac{7}{12}\right)\,. \tag{6.78}$$

6.3.10 Comparison

Now we are in the position to depict qualitatively how the lower and the upper critical field $B_{\mathrm{c1}}(\kappa)$ and $B_{\mathrm{c2}}(\kappa)$ from (6.78) and (6.37) depend on the Ginzburg-Landau parameter κ in form of Fig. 6.11a). There we show also the dependence of the numerically determined $B_{\mathrm{c1}}^{\mathrm{real}}(\kappa)$ from κ. Thus, one recognizes that $B_{\mathrm{c1}}(\kappa)$ turns out to be a quite good approximation for $\kappa \geq 3$.

6.3.11 Example

In order to provide an illustrative example, we determine the critical fields for the high T_{c}-superconductor $YBa_2Cu_3O_7$, which is characterized by the Ginzburg-Landau parameter $\kappa = 100$ and the London penetration length $\lambda_{\mathrm{L}} = 200\,\mathrm{nm}$. At first we calculate the lower critical field (6.78) by taking into account the flux quantum (4.100):

$$B_{\mathrm{c1}} = \frac{\phi_0}{4\pi\lambda_{\mathrm{L}}^{2}}\left(\ln\kappa+\frac{7}{12}\right) = 21\,\mathrm{mT}\,. \tag{6.79}$$

Then we compare that with the corresponding upper critical field (6.37) by taking into account (6.78):

$$B_{\mathrm{c2}} = B_{\mathrm{c1}}\,\frac{2\kappa^{2}}{\ln\kappa+7/12} = 81\,\mathrm{T}\,. \tag{6.80}$$

Thus, for an extreme type II superconductor B_{c1} is much smaller than B_{c2}. This means that there is a huge range of magnetic induction, in which flux quanta exist in the Shubnikov phase.

a) 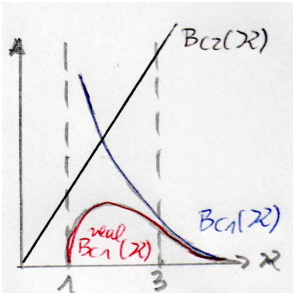

b) 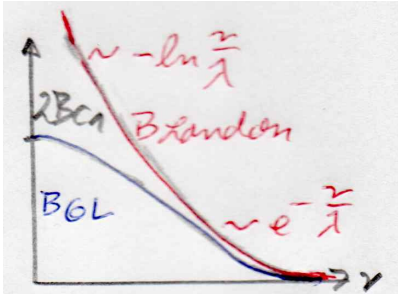

Figure 6.11: a) Lower and upper critical field (6.78) and (6.37) as well as numerically determined $B_{c1}^{real}(\kappa)$ as function of Ginzburg-Landau parameter κ. b) Spatial profile of magnetic induction near flux quantum.

6.3.12 Remark

In the preceding discussion we did not yet clarify how the magnetic induction behaves at the center of the flux quantum. To this end one has to solve the Ginzburg-Landau equations numerically. The result is that the magnetic induction at the core of the flux quantum turns out to be precisely twice the lower critical field, see Fig. 6.11b):

$$B(0) = 2B_{c1}\,. \tag{6.81}$$